IOSR Journal of Biotechnology and Biochemistry (IOSR-JBB)
ISSN: 2455-264X, Volume 2, Issue 1 (Jan. – Feb. 2016), PP 19-34
www.iosrjournals.org

Experimental (FT-IR, UV-visible, NMR) spectroscopy and molecular structure, global reactivity parameter, Fukui function, NBO, NLO, HOMO-LUMO, MESP and QTAIM analyses of Abacavir using density functional theory

Shashi Kumar Gangwar, Ambrish Kumar Srivastava and R.B. Singh*
Department of Physics, University of Lucknow, Lucknow-226007, Uttar Pradesh, India

Abstract: *In the present work, FT-IR, ^1H NMR, UV-visible spectra of [(1S,4R)-4-[2-amino-6-(cyclopropylamino) purine-9-yl]cyclopent-2-en-1-yl] methanol (Abacavir) have been analyzed at the room temperature. The equilibrium geometry, harmonic vibrational frequencies, infrared intensities, ^1H-NMR and bonding properties have been calculated by density functional theory employing B3LYP hybrid exchange-correlation functional with complete relaxation in the potential energy surface. The fundamental vibrational modes have been assigned on the basis of the potential energy distribution. The theoretically predicted vibrational wave-numbers have shown a very good agreement with experimental data of the molecule by proper scaling. The natural bond orbital (NBO) analysis is used to predict the chemical interpretation of hyper-conjugative interactions and electron density transfer between occupied (bonding and lone pair) orbital to unoccupied (anti-bonding) or charge delocalization. The energies and oscillator strengths are calculated by time dependent density functional theory and found to be in agreement with the experimental values. The local reactivity descriptors; Fukui function (f_k^+, fk^-), local softness (s_k^+,s_k^-) and electrophilicity indices (ω_k^+,ω_k^-) have been used to determine the reactive sites within the molecule. The first hyperpolarizabilty (β_0) of abacavir is found to be16.62×10^{-30}esu indicating its non linear optical (NLO) behavior.*

Keywords: *DFT, hydrogen bonding, HOMO-LUMO, QTAIM, Fukui function, MEP surface analysis, NLO analysis.*

I. Introduction

A large number of structural nucleoside analogous (NA) have been designed and synthesized [1, 2] for anticancer activity [3] and viral infections. Several derivatives of abacavir [4] have shown potent antiviral activity [(1S,4R)-4-[2-amino-6-(cyclopropylamino)purine-9-yl]cyclopent-2-en-1-yl] that have occupied an important position among these antiviral agents and this is used either singularly or in combination with other drugs for the treatment of human immunodeficiency virus (HIV) and aids.[5] Abacavir is a strong class nucleoside analog reverse transcriptase inhibiter (NRTI) used for the treatment of the cancer HIV and AIDS (the formation of DNA from an RNA Template) [6-8]. It has been seen that 5-substituted-2-deoxyuridines reduces cancer cells proliferation by inhibiting thymidylate synthase, an enzyme essential in the synthesis of DNA [9]. Potent anticancer agents have been recently synthesized in which the cyclopentene ring is replaced by an indane system [10] and assayed on different cancer cell lines. The title compound shows more resistance to hydrolases than that of the natural nucleosides. The charged transfer involved in the formation of adducts is also qualitatively studied [11]. However, nucleoside anticancer drug, commonly associated with various adverse effects, are associated with the molecular structure [12]. The anticancer drug and DNA binding mechanism are involved in the donation of electrons from DNA and acceptance of the electrons by the drug molecule. Molecule's structural studies, along with the vibrational spectroscopic studies, are the patent tools to study the active sites, as well as, the adverse effects [13].

We have carried out a detailed quantum chemical investigation on abacavir. Density functional theory (DFT) is one of the most popular quantum chemical method, which has been used in a number of studies in the systems of biological and pharmacological importance [14-17]. The quantum chemical descriptors based on density functional theory are found to be useful in several QSAR Studies [18, 19]. The vibrational modes are assigned depending on their potential energy distribution (PED) and H–bondings with the use of the quantum theory of atoms in molecules (QTAIM) [20-21]. The natural bond analysis has been carried out in order to study the intra-molecular bonding, interactions among bonds and delocalization of unpaired electrons. The UV absorption spectrum was examined in chloroform solvent and compared with the calculated one in gas phase, as well as in solvent environment, using TD-DFT/ PCM approach. The ^1H chemical shifts are calculated using IEFPCM model and gauge independent atomic orbital (GIAO) approach in the appropriate solvent. In order to compare the ^1H NMR chemical shifts, the correlation graph between the experimental and calculated chemical shifts has been drawn. The highest occupied molecular orbital (HOMO) and lowest unoccupied molecular

orbital (LUMO) analyses have been carried out to support and clear the information pertaining to charge transfer (CT) within the molecule. In recent years, DFT predicted reactivity descriptors namely, global hardness (η), chemical potential (μ), electro-negativity (χ), electrophilicity index (ω), fukui function (f_k^+,f_k^-), philicity (ω^+) etc have been extensively explored . The electrophilicity and philicity [22] indices have successfully been used to determine the biological activity and toxicity property of different organic compounds. The molecular electrostatic potential (MESP) surface and natural bond orbital analysis is used for predicting binding sites and relative reactivity towards electronphilic attack and in studies of biological recognition and hydrogen bonding interactions, of abacavir has also been analyzed.

II. Experimental details

The FT-IR spectrum was recorded in KBr medium on Bruker spectrometer. The ^{1}H NMR spectrum was recorded in MEOD on Bruker DRX-300 spectrometer using TMS as an internal reference. The UV-visible absorption spectrum (1×10^{-5}M solution in chloroform) was recorded on ELICO SL-164 spectrophotometer.

III. Quantum chemical calculations

All the quantum chemical calculations are carried out with the help of Gaussian 09 code [23] for the prediction of the molecular structure, energies of the optimized structure, ^{1}H NMR chemical shifts, NBO analysis, vibrational wavenumbers, uv analysis, reactivity descriptors and first hyper-polarizability using B3LYP functional and 6-311++G(d,p) basis set [24] which invokes Becke's three parameter (local, nonlocal, Hartree-Fock) hybrid exchange functional (B3) with Lee-Yang-Parr correlation functional (LYP),The basis set 6-311++G(d,p) with 'd'polarisation functions on heavy atoms and 'p' polarization functions on hydrogen atoms are used for better description of polar bonds of molecule [25]. In a recent study, B3LYP method has been found to be better than MP2 method [26]. It should be emphasized that 'p' polarization functions on hydrogen atoms. Time dependent density functional theory (TD-DFT) is used to find the various electron excitations and their nature within the molecule. The optimized geometrical parameters are used in the vibrational wave numbers calculation to characterize all stationary points as minima and their harmonic vibrational wave numbers are positive. Potential energy distribution along internal co-ordinate is calculated by Gar2ped software [27].

IV. Results and discussion

Molecular structure and Optimized geometry

The optimized geometry for ground state lower energy conformer is shown in figure 1. Selected optimized parameters of the title compound calculated at B3Lyp/6-311++ G (d,p) are listed in the Supplementary Table S2.The molecule posses C_1 symmetry and total energy for the ground state lower energy conformer is calculated -948.29 a.u. and the dipole moment about the symmetry is 1.2713 debye. The common structure of molecule include one cyclohexane ring, one pyrimidine ring one cyclopentene ring and one cyclopropane ring in 3d geometry in which R1 ring is attached with NH_2 group and OH group is attached with cyclopentene through CH_2. The bond length bond angle and dihedral angles are calculated for the equilibrium state of the abacavir. The molecules are packed into parallel to (2,1,1) and unit cell dimensions (a=9.19,b=13.70,c=11.60,α=90°,β=109.09,γ=90°) [Drug id-EP2242758] plane. The layers are 2.20 A° apart. They are not exactly planner. The molecules are slightly tilted with respect to the mean position.

QTAIM analysis

The quantum theory of atoms in molecule (QTAIM) defines the chemical bonding and structure of the chemical system based on the topology of the electron density. In addition to bonding, QTAIM allows the calculation of certain physical properties on a per atom basis, by dividing space up into atomic volumes containing exactly one nucleus which acts as a local attractor of the electron density(ED). Molecular graph of using AIM program at B3LYP/6-311++G (d,p) level is shown in Figure (6). Topological as well as geometrical parameters for bonds of interacting atoms in abacavir are given in Table 6. For the interaction N6….H29, ED ($\rho_{N6.....H29}$) and its Laplacian ($\nabla^2\rho_{bcp}$) follow the Koch and popelier criteria and distance between interacting atoms ($D_{N6.....H29}$ = 2.45) is less than the sum of vander Waals radii of these atoms ($r_N + r_H$ =2.643 A°). Therefore, intramolecular interaction N6-H29 is a hydrogen bond. The various inter-molecular, intra-molecular interactions and H–bonding are characterized with the use of the quantum theory of atoms in molecules (QTAIM) [28]. H-bonded interactions may be classified as follows:

(i) Strong H–bonds are characterized by $\nabla^2\rho$ ($_{BCP}$) < 0 and H_{BCP}< 0 and their covalent character is established.

(ii) Medium H–bonds are characterized by $\nabla^2\rho$ ($_{BCP}$) > 0 and H_{BCP} < 0 and their partially covalent character is established.

(iii) Weak H–bonds are characterized by $\nabla^2\rho_{(BCP)} > 0$ and $H_{BCP} > 0$ and they are mainly electrostatic.

Other weak interactions (X⋯Y) are characterized by $\nabla^2\rho_{(BCP)} > 0$ and $H_{BCP} > 0$.The nature of N6-H29 Hydrogen bond is week due to $\nabla^2\rho_{(BCP)} > 0$ and $H_{BCP} > 0$. Espinosa proposed a proportionality between hydrogen bond energy (E_{HB}) and potential energy density (V_{BCP}) at N.....H contact, $E_{HB} = ½(V_{BCP})$ [29-30]. According to this equation the energy of N6-H29 hydrogen bond is calculated as -2.38kcal/mol.

Vibrational analysis

The selected theoretical and experimental vibrational modes of title molecule**,** calculated at B3LYP/6–311++G(d,p) method and their assignments using PED are given in Table 3. Comparison between theoretical and experimental IR spectra in the region 4000–400 cm^{-1} is shown in Figure 5. Two factors may be responsible for the discrepancies between the experimental and computed wavenumbers. The first is caused by the environment (gas and solid phase) and the second is due to the fact that the experimental values are an anharmonic wavenumbers while the calculated values are harmonic ones. Therefore, calculated wavenumbers are scaled down using scaling factor 0.9608 to discard the anharmonicity present in real system. The Vibrational band assignments have been made on the basis of normal co-ordinate analysis. Internal coordinates have been chosen according to Pulay's recommendations. Gauss-View program is also used to assign the calculated harmonic vibrational wavenumbers.

N–H Vibrations

In the FT-IR spectrum of Abacavir, the N-H stretch of (ν_{NH2}) is observed at 3467 cm^{-1}, whereas this is calculated as 3562 cm^{-1}. The weak band of NH_2 scissoring is assigned at 1625-1597 cm^{-1}, corroborate well with the observed mode at 1630-1590 in FT-IR spectrum. The observed NH wagging mode at 550cm^{-1} agrees well with the calculated wavenumber at 535 cm^{-1}. The observed NH_2 wagging mode at 812 cm^{-1} agrees well with the calculated wavenumbers at 803 cm^{-1}.

C–H and O–H Vibrations

The stretching modes of CH in cyclopropane ring are observed in the region 3104 -2869cm^{-1} and one OH group is attached with cyclopropane ring observed frequency to be 3345. Rocking mode of methylene is observed at 1325 cm^{-1}, whereas it is calculated to be 1333 cm^{-1}.The aromatic structure shows the presence of C–H stretching vibration in the region 3100-3303 cm^{-1}, which is the characteristic region for the ready identification of C-H stretching vibration.

C-C Vibrations

In aromatic hydrocarbon, skeletal vibrations involving carbon–carbon stretching within ring are absorbed in the region 1225-1630 cm^{-1}. The wavenumber calculated at 1232-1625 cm^{-1} assigned to the C=C stretches in pyrimidine ring which corroborate well with experimental at 1530-1532 cm^{-1}. Rocking of C–C bond is calculated at 1546 cm^{-1} and observed in the experimental spectrum with weak intensity.

C–O Vibrations

The experimental FT–IR spectrum gives C-O mode at 962cm^{-1}. The "C–O stretching vibrations" of alcohol group actually consists of two asymmetrical coupled vibrations as O−H=O−H, O−C−H−H and these bands occur in the region 1536–1113 cm^{-1}. The calculated wavenumber at 1010 cm^{-1} with 16% contribution in PED demonstrates to the O–C–C stretching vibration ($\nu_{O1–C19}$) and corresponds to the observed wavenumber at 962 cm^{-1} experimentally. In theoretical IR spectrum, a combination band of the O−C=O−C stretching vibration ($\nu_{C19–O1}$)' and C–C–H deformation' at 1235 cm^{-1} is observed at same wavenumber in experimental FT–IR spectrum.

C=C Vibrations

The calculated C=C stretches of R_3 pyrimidine at 1543-1646 cm^{-1} matches well with the reported band in literature in the region 1530–1630 cm^{-1}. The C=C stretches of R_3 pyrimidine Ring are assigned at 1570, 1630, 1530cm^{-1}, whereas these DFT modes are observed at 1630, 1625, 1532 cm^{-1}, respectively in FT–IR spectrum. In DFT calculation, a band at 869 cm^{-1} displays the pyrimidine ring deformation (δ–R2) with 16 % contribution in PED and corresponds to the observed wave number 988cm^{-1}. The calculated C–C–C deformation associated with pyrimidine ring at 1333 cm^{-1} agrees with the observed wavenumber at 1325 cm^{-1}.The ring puckering vibration (a tortional mode) associated with pyrimidine is assigned at 754 cm^{-1} and appears at same wave number in FT–IR spectrum. The asymmetric deformation mode of pyrimidine ring (δ_{as}–R1) assigned at 754cm^{-1} agrees with the observed band at 748 cm^{-1}, experimentally.

C=N and C–N Vibrations

The calculated band at 1347 cm^{-1} is assigned to the stretching vibration of Schiff base $\upsilon_{C=N}$ mode and calculated band at 1355 cm^{-1} for $\upsilon_{C=N}$ also matches well with the reported band at 1647 cm^{-1} in literature. The observed C–N stretching vibration as ν_{C18-N4} at 1225 cm^{-1} matches well with the calculated wave number at 1232 cm^{-1}. The C–N stretching vibration is also active in the region 1275 ± 55 cm^{-1}, reported in literature.

UV–Visible spectroscopy

The nature of the excitations in the experimental UV–Visible spectrum of (**1**) has been studied by the time dependent density functional theory (TD–DFT) [31-32]. The calculated and experimental electronic excitations of high oscillatory strength are listed in Table 1. The experimental UV–Visible spectrum of abacavir is also shown in Figure 3. Frontier molecular orbitals *i.e.* the highest occupied molecular orbital (HOMO) and lowest unoccupied molecular orbital (LUMO) are very popular quantum chemical parameters. They determine the molecular reactivity and ability of a molecule to absorb light. The vicinal orbitals of HOMO and LUMO [33] play the same role of electron donor and electron acceptor, respectively. HOMO–LUMO and their vicinal molecular orbital plots involved in the high oscillator strength electronic excitations of abacavir are shown in Figure 4. The HOMO–LUMO energy gap is an important stability index. The HOMO–LUMO energy gap of 5.0912eV for abacavir**,** calculated at B3LYP/6–311++G (d, p) method reflects the chemical stability of the molecule.

A combined experimental and theoretical UV–Visible spectrum analysis of abacavir indicates that the first observed electronic excitation at λ_{max} = 306 nm agrees with the calculated electronic excitations at λ_{max} = 283.86 nm, f = 0.3474. The second observed electronic excitation at λ_{max} = 306 nm corresponds to the calculated electronic excitations at λ_{max} = 247.78 nm, f = 0.0823.Therefore, the observed λ_{max}=246 values are blue shifted up to ~2 nm compared with the calculated λ_{max} in the theoretical UV–Visible spectrum. According to TD–DFT calculations the bands at 283.86, 247.78 nm originate mainly due to H→L+7, H→H+6 excitations, respectively. The molecular orbital H is localized over oxygen atom of hydroxy group, whereas H→H+3, H→H+3, L→L+1 are localized over C17–C18 of Schiff base, C13–C12 and C16–N5 of pyridine ring, respectively. A combined molecular orbital coefficients and molecular orbital plots analysis assigns the nature of these electronic excitations H→L, H→L+7, H→H+6 excitations as n(O19)→π^*(C10O11),n(O19)→π^*(C20C21), n(O19)→π^*(C15N16), respectively. Therefore, nature of both the observed electronic excitation is n→π^*.

^{1}H NMR Spectroscopy

The observed ^{1}H NMR spectrum of the studied compound is given in the Supplementary material.The geometry of the studied compound, together with that of tetramethylsilane (TMS) is fully optimized. ^{1}H NMR chemical shifts are calculated with GIAO approach at B3LYP/6–311++G (d,p) method. Chemical shift of any 'x' proton (δ_X) is equal to the difference between isotropic magnetic shielding (IMS) of TMS and proton (x). It is defined by the equation: $\delta_X = IMS_{TMS} - IMS_X$.The correlation value ($r^2$ = 0.81) shows that there is a good agreement between experimental and calculated chemical shifts. The NH_2 group hydrogen attached at six membered pyrimidine ring appears as doublet at 6.489-6.501 ppm due to nitrogen inversion. The -N=CH- peak observed at 10.920 as singlet due to the attachment of Nitrogen atom. This peak show downfield shift then NH_2 group. The hydrogen peaks of methyl group (C-H) observed at 7.2118-8.731the primary alcoholic group observed at 5.341 ppm due to the intermolecular hydrogen bonding with the solvent molecule. The singlet chemical shifts have been observed in the case of theoretical calculated ^{1}H NMR spectrum. This is due to the fact that single molecule is involved in the gas phase calculation.^{1}H NMR chemical shifts are calculated with GIAO approach at B3LYP/6–31G (d,p) method. The calculated and experimental^{1}H NMR chemical shifts (δ / ppm) of abacavir are given in Table 2. In order to compare the chemical shifts, correlation graph between the experimental and calculated ^{1}H NMR chemical shifts is shown in Supplementary material (S Figure 1). In the ^{1}H NMR spectrum of title compound, a quartet chemical shift in range 7.218–7.859 ppm and in range 8.071–8.731 ppm designate presence of the $–CH_2$, $–CH_3$ group, respectively. The observed singlet chemical shifts at 7.557 triplet chemical shift at 10.920-10.452ppm for Schiff base –CH=N and proton peaks of cyclopropane ring, respectively indicates formation of N-(1,2,3-trimethylcyclopropyl)-2,5-dihydropyrimidin-5-amine(–CH=N–NH–C3H6) in the title molecule. The correlation graph follows the linear equation: y = 1.2037 x –1.0791, where 'x' is the calculated ^{1}H NMR chemical shift, 'y' is the experimental ^{1}HNMR chemical shift (δ in ppm). The correlation value (R = 0.9451) shows that there is good agreement between experimental and calculated ^{1}H NMR chemical shifts.

Chemical reactivity

Here the chemical reactivity of molecule can be described in two ways as: (i) using molecular electrostatic potential (MESP) map (ii) Global and local electronic reactivity descriptors.

Molecular electrostatic potential (MESP) map

The molecular electrostatic potential (MESP) map is widely used as a reactivity map to display the most probable regions for electrophilic / nucleophilic attack of charged point–like reagents on organic molecules. The negative electrostatic potential corresponds to an attraction of the proton by the concentrated electron density in the molecule (red color on the MESP surface), whereas the positive electrostatic potential corresponds to repulsion of the proton by atomic nuclei in regions where low electron density exists and the nuclear charge is incompletely shielded (blue color on the MESP surface) [34-35]. In the present study, MESP map of abacavir is shown in Figure 8. Actually, MESP map is an electron density isosurface on which molecule's electron density has a particular value and that encloses a specified fraction of the molecule's electron probability density. The electrostatic potential at the different points on the electron density isosurface is shown by coloring the isosurface with contours. The different values of electrostatic potential at the surface are represented by different colors as red represents the region of most electronegative electrostatic potential, blue represents region of most positive electrostatic potential and green represents region of zero potential. Electrostatic potential increases in the order red < orange < yellow < green < blue. The color code of MESP map is in the range between -5.049×10^{-2}a.u. (deepest red) to $+5.049 \times 10^{-2}$ (deepest blue). The regions of negative electrostatic potential [33] are usually associated with lone pair of electronegative N and O atoms.

It can be seen from the MESP map of abacavir that the decrease in the positive electrostatic potential around O-H group and negative electrostatic potential around N4, N6 nitrogen atom of pyridine ring N–H indicates the equalization of electrostatic potentials and responsible for the intramolecular hydrogen bonding N6···H29. The ESP map shows negative potential regions merely over the O1 as a red blob; N5, N6, O1 as orange blob and N4, N3 as a yellowish blob, whereas positive potential region as a deep blue blob over the N2, H31 hydrogen atom of cyclopropane ring of molecule. Therefore, these N and O atoms in abacavir are act as proton donor due to presence of free loan pair of electron and form intermolecular hydrogen bonding or vander-waals interactions as (N/O···H–N) with proton acceptors (H–N) group of various amino acids present in the living system. In same manner, proton acceptor (C12–H29) group of title molecule forms intermolecular hydrogen bonding or Vander-waals interactions as (N6–H29···O) with proton donor oxygen atom of amino acids. Thus, electrostatic potential play a key role to explain the interaction of investigated abacavir molecule with biomolecules as proteins present in the living system.

Local reactivity descriptors

Selected electrophilic reactivity descriptors (f_k^+, s_k^+, ω_k^+) and nucleophilic reactivity descriptors (f_k^-, s_k^-, ω_k^-) for the title compound**,** using Mulliken atomic charges are given in Table (4). The maximum values of local electrophilic reactivity descriptors (f_k^+, s_k^+, ω_k^+) at benzene ring carbonC16of the title compound indicates that this is the most electrophilic site. The nucleophilic reactivity descriptors (f_k^-, s_k^-, ω_k^-) analysis of the title compound shows that N1 is the most nucleophilic site. Therefore, the nucleophilic attack of N1 site of the compound at the most electrophilic site C16 confirms the formation of the product molecule attached with cyclopropane ring through nitrogen atom in the title molecule. The maximum values of local electrophilic reactivity descriptors (f_k^+, s_k^+, ω_k^+) at 1,3-dimethylidazolidine carbon (C20) of abacavir indicate that this site is more prone to nucleophilic attack and favors formation of the new unsymmetrical dimer by attack of 2–unsubstituteddimethylidazolidine nucleophile at (C20). In same way, the maximum values of nucleophilic reactivity descriptors (f_k^-, s_k^-, ω_k^-) at nitrogen atom of –CH=NH–CH part of molecule (N1) indicate that this site is more prone to electrophilic attack.

Global reactivity descriptors

Electro-negativity (χ), the negative of chemical potential (μ) [36] and hardness (η) [37-38] are respectively given by,

$\chi = -½ (\varepsilon_{LUMO} + \varepsilon_{HOMO})$ (1)

$\mu = -\chi = ½ (\varepsilon_{LUMO} + \varepsilon_{HOMO})$ (2)

$\eta = ½ (\varepsilon_{LUMO} - \varepsilon_{HOMO})$ (3)

Using μ and η, Parr et al. have proposed a new quantum chemical descriptor, electrophilicity index (ω) which measures the tendency to absorb electrons and is defined as-

$\omega = \mu^2/2\eta$ (4)

And the global softness is the reciprocal of the hardness, given as-

$S = 1/2\eta$ (5)

Maximum electronic charge have been calculated using-

$\Delta N_{max} = -\mu / \eta$ (6)

The condensed fukui function (ff) are calculated as follow.

$f^+ = \frac{1}{\Delta N}[q_k(N_0+\Delta N) - q_k(N_0)]$ (for nucleophilic attack) (7)

$f^- = \frac{1}{\Delta N}[q_k(N_0) + -q_k(N_0-\Delta N)]$ (for electrophilic attack) (8)

Electrophilicity reactivity index measures the stabilization in energy when the system acquires an additional electronic charge (ΔN_{max}) from surrounding. The electrophilicity index (ω) is positive, definite quantity and the direction of the charge transfer is completely determined by the electronic chemical potential (μ) of the molecule because an electrophile is a chemical species capable of accepting electrons from the surroundings and its energy must be reduce on accepting electronic charge. Consequently, its electronic chemical potential must be negative.

Natural bonding orbital's (NBO) analysis

Natural bond orbital calculation has been carried out in the order to investigate intra molecular charge transfer interactions, delocalization of electron density and rehybridisation [39-40]. in the molecule. The orbital interactions were analyzed on the basis of natural bond analysis the electronic wave functions are interpreted in terms of a set of occupied Lewis type (bonds and lone pair of e^-)set of unoccupied non Lewis (antibonds and Rydberg) localized NBO orbital's. Delocalization of the electron density (ED) between these orbitals corresponds to a stabilizing donor-acceptor interaction. The delocalization effects (donor-acceptor ,charge transfer into the molecular orbitals) can be estimated from off –diagonal elements of the Fock matrix in the nbo basis for each donor (i) and acceptor (j), the stabilization energy E^2 associated with the delocalization i, j is estimated.

In order to characterize the intra-molecular interactions quantitatively, a second–order perturbation theory is applied that gives the energy lowering associated with such interactions. The π–conjugation and resonance due to π–electron delocalization in ring is involved due to the π→π* interactions, whereas the primary hyperconjugative interactions due to the various types of orbital overlaps such as $\sigma\rightarrow\pi^*$, $\pi\rightarrow\sigma^*$, $n\rightarrow\sigma^*$ and secondary hyperconjugative interactions due to the $\sigma\rightarrow\sigma^*$ orbital overlap [47].Second–order perturbation theory analysis of the Fock matrix in NBO basis for abacavir is presented in Table 5. The interactions π(N6–C21)→π*(N5–C16), π(N6–C21)→π*(C17–C18) and π(C17–C18)→π*(N6–C21), π(C17–C18)→π*(N5–C16), n_1(N5)→π*(C16–C18) / π*(N6–C21) are responsible for the conjugation of respective π–bonds in pyrimidine ring. The high electron density at the conjugated π bonds (1.77385–1.64835) and low electron density π* bonds (0.45608–0.45356) of pyrimidine ring indicate strong π–electron delocalization within ring leading to a maximum stabilization of energy ~36.35kcal/mol. The interactions π(C2–C3)→π*(C6–C7), π(C6–C7)→π*(C2–C3) are responsible for the conjugation of bonds C2–C3, C6–C7 with C2–C6 and stabilized the molecule with maximum energy ~18.64 kcal/mol. In same manner, the interactions π(N4–C20)→π*(C16–N18), π(C17–N18)→π*(N4–C20), n(N3)→π*(C17–C18)demonstrates the conjugation of these bonds with C17–C18 in five membered ring R2. It is to be noticed that the charge transfer interactions are formed by the orbital overlap between bonding (π) and antibonding (π*) orbitals, which results in intramolecular charge transfer (ICT) causing stabilization of the system. The movement of π–electron cloud from donor to acceptor *i.e.* intramolecular charge transfer (ICT) can make the molecule more polarized, which is responsible for the NLO properties of molecule. Therefore, the titled compound may be used for non–linear optical materials. The primary hyper-conjugative interaction π_1(C8–N9)→σ*(N1–H26) designates the intramolecular hydrogen–bonding as N1–H26···N9. The primary hyperconjugativeinteractionsn_1(N9)→σ*(C7–C8), n_2(O11)→σ*(C10–O12), n_2(O19)→σ*(N17–C18) / σ*(C18–C20) and other interactions n_2(O12)→π*(C10–O11), n_1(N17)→π*(C15–N16) / π*(C18–O19) are stabilized the molecule to a greater extent ~50.54kcal/mol. The secondary hyper-conjugative interactions associated with pyrimidine ring such as σ(N4–C20)→σ*(C16–C18), σ(N4–C20)→σ*(C17–C18), σ(N6–C21)→σ*(C17–C18) and associated with 1,3-dimethylimidazolidine ring as σ(N4–C20)→σ*(C17–C18), σ(C17–C18)→σ*(N3–C11) are stabilized the molecule with maximum energy ~5.49kcal/mol.

Selected Lewis orbitals (occupied bond or lone pair) of abacavir with their NBO hybrids are listed in Table 6. The valence hybrids analysis of NBO orbitals shows that all the N–H / C–N bond orbitals are polarized towards the nitrogen atom (ED = 57.41 – 74.62 % at N), whereas C–O bond orbitals towards oxygen atom (ED = 64.94 – 68.75 % at O). The electron density distribution (occupancy) around the imino group (>N–H) and loan pair around electronegative atoms mainly influences the polarity of the compound. Therefore, they consist with the maximum electron density on the oxygen and nitrogen atoms, which is responsible for the polarity of molecule.

Static dipole moment (μ_0), mean polarizability ($|\alpha_0|$), anisotropy of polarizability ($\Delta\alpha$) and first hyperpolarizability (β_0)

In order to investigate the relationship between molecular structure and NLO response, first hyperpolarizability (β_0) of this novel molecular system, and related properties ($|\alpha_0|$ and $\Delta\alpha$) are calculated using B3LYP/6–31G(d,p), based on the finite–field approach and their calculated values are given in Table 6.

Total static dipole moment (μ_0), mean polarizability ($|\alpha_0|$), anisotropy of polarizability ($\Delta\alpha$) and first hyperpolarizability (β_0), using x,y,z components are defined as.

$\mu_0 = (\mu^2_x + \mu^2_y + \mu^2_z)^{1/2}$

$|\alpha_0| = 1/3(\alpha_{xx} + \alpha_{yy} + \alpha_{zz})$
$\Delta\alpha = 2^{-1/2}[(\alpha_{xx} - \alpha_{yy})^2 + [(\alpha_{yy} - \alpha_{zz})^2 + (\alpha_{zz} - \alpha_{xx})^2 + 6\ \alpha^2_{xx}\ ]^{1/2}$
$\beta_0 = [(\beta_{xxx} + \beta_{xyy} + \beta_{xzz})^2 + (\beta_{yyy} + \beta_{xxy} + \beta_{yzz})^2 + (\beta_{zzz} + \beta_{xxz} + \beta_{yyz})^2]^{1/2}$

Large value of particular component of the polarizability and hyperpolarizability indicate a substantial delocalization of charge in these directions. Since the value of the polarizability ($|\alpha_0|$), first hyperpolarizability (β_0) of Gaussian 09 output are reported in atomic unit (a.u.) and these values are converted into electrostatic unit (esu) using converting factors as (for α_0: 1a.u. = 0.1482 x10^{-24}esu; for β_0: 1a.u = 0.008639 x10^{-30}esu). The first hyperpolarizability (β_0) of the title compound is calculated as 16.62 x10^{-30} esu [40]. In this study, p–Nitroaniline (p–NA) is chosen as a reference molecule because there were no experimental values for the title compound. The p–NA is one of the prototypical molecules used in the study of the NLO properties of molecular systems (for p–NA, β_0 = 11.54 x10^{-30} esu). Therefore, investigated molecule will show non–linear optical response and might be used as non–linear optical (NLO) material.

V. Conclusions

A systematic study has been conducted on the structural and spectral analysis of non linear moleculeabacavir by spectroscopic methods and quantum chemical calculations. The Vibrational and structural study of title compound using various spectroscopic techniques authenticates that the calculated theoretical and observed FT-IR, UV and ^{1}H NMR chemical shifts are in good agreement with the observed data. A combined experimental and theoretical UV–Visible spectral analysis indicates that both observed wavelength absorption maxima (λ_{max}) have blue shifts up to ~27 nm compared with the calculatedλ_{max} values and their nature is assigned as $n\rightarrow\pi^*$ using molecular orbital coefficients analysis and molecular orbital plots. NBO analysis shows that the interaction π_1(C8–N9)→σ*(N1–H26) is responsible for intra molecular hydrogen–bonding N1–H26···N9 and the interactions $n\rightarrow\sigma^*$, $n\rightarrow\pi^*$ stabilizes the molecule to a greater extent ~50.54kcal/mol. The red shift in the wave number of both proton donor as pyrimidine (N–H)and proton acceptor as *C–N* confirms the presence of the hydrogen bonding N6–H29. AIM calculation also confirms presence of the intermolecular interaction N6–H29 due to the existence of the bond critical point at H29 contact. On the basis of topological and geometrical parameters, it has been found that the interaction N6–H29 is a weak hydrogen bond due to $\nabla^2\rho_{BCP} > 0$ and $H_{BCP} > 0$. The result of hydrogen bonding is also noticeable in ESP map due to the absence of blue color relative to the benzene ring attached with N–H proton. The electrostatic potential (ESP) map shows negative potential (red region) merely over the hydroxyl group oxygen atoms as O1, whereas positive potential (blue region) over the N7 hydrogen atom and primary amine (N2-C8-C16-H31) of abacavir. The global electrophilicity index (ω = 1.38eV) shows that title molecule behaves as a strong electrophile. The electrophilic reactivity descriptor (f_k^+, s_k^+, ω_k^+) analysis for title molecule indicates that the investigated molecule might be used as a precursor for the target synthesis of new unsymmetrical derivatives of the title compound. The compound exhibits strong effective intramolecular charge transfer (ICT) due to movement of π–electron cloud from donor to acceptor, which is responsible for polarity and shows non–linearity. The first hyperpolarizability (β_0 = 16.62 x10^{-30}) shows that compound can be used as material for non–linear optical (NLO) applications.

Acknowledgement

Authors are thankful to the Department of Chemistry, University of Lucknow, Lucknow for providing the computational facility and A.K Srivastava is thankful to Council of scientific and industrial Research (CSIR), New Delhi, India for providing a research fellowship via grant no.09/107(0359)/2012-EMR-I.

References

[1]. B.D. Cheason, M.I. Keating, W. Plunkett (1997) Nucleoside analogous in cancer therapy. Dekker, New York.
[2]. P. Sarmah, R.C. Deka Anticancer activity of nucleoside analogues J Mol Model (2010) 16:411-418.
[3]. J. Jacquesn, L.B.H.Lorraine, O.France, Sylvain BAR, Herriette G (2003) cancer Chemother Pharmacol 52:497-506.
[4]. P. Sarma , C.Ramesh J. Deka J Mol Model (2010) 16:411-418.(doi 10.1007/s00894-009-0551-9.
[5]. A Carr, C Workman, D.E. Smith, J Hoy, J. Hudson Jama, 2002.
[6]. F. Fermandez , X. Garcia-Mera,Morales M. Mera Morales, Rodriguez-Borges JE(2001) Synthesis 2:239-242.
[7]. F. Abad, Alvarez. F. Alvarege, F. Fermandez, X.Garcia-Mera, J.E. Rodriguez-Borges (2001) Nucleosides. Nucleic Acids 20:1127-11228.
[8]. S.W. Yao, V.H.C.Lopes, F. Fermandez, X. Garcia-Mera , M. Morales, Rodrguez-Borges JE, Cordeiroa MNDS (2003) Bioorg Med Chem 11:4999-5006.
[9]. C.Marlon, C.H Lee, G A. Gfesser, K. Erol, S. Bayburt, A.O. Shripad, Stewart, Yu Haixia Bioorganic & Medicinal Chemistry Letter 11 (2001) 83±86.
[10]. S.W. Yao, V.H.V. Lopes, F. Fermandez, X. Garcia-Mera, Morales, J.E. Rodriguez-Borges, M.N.D.S Cardrorroa (2003) Bioorg Med Chem 11:4999-5006 (ichiro hayakawa, rieko shioya t J. Wan, L. Zhang , G.F. Yang (2004) J Compute Chem 25:1827-1882.
[11]. H.K. Srivastava,F.A. Pasha , P.P. Singh (2005) Int J Quantum Chem 103:237-245.
[12]. A.M. Helguera, J.E Rodriguez-Borges, X. Garcia-Mera , F. Fermandez , M.N.D.SCardeiroa (2007) J Med Chem 50:1537-1545.
[13]. A. Carr, A. David, Cooper (2000)(doi :10.1016/SO140-6736(00)02854-3
[14]. A.K. Srivastava, B. Narayana, B.K. Sarojini, N. Misra, Indian J. Phys. 88 (2014) 547– 556.
[15]. A.K. Srivastava, V. Baboo, B. Narayana, B.K. Sarojini, N. Misra, Indian J. Pure Appl. Phys. 52 (2014) 507–519.

[16]. A.K. Srivastava, N. Misra, Can. J. Chem. 92 (2014) 234–239.
[17]. A.K. Srivastava, N. Misra, Chem. Phys. Lett. 612 (2014) 302–305.
[18]. P. Zbigniew , G. Jean-Luc G, W. Cathey E, Guangvi (2001) Nucleosides Nucleotides Nucleic Acids 20:323-328.
[19]. K.Fukui , T.Yonezawa ,H. Shingu (1952) J Chem Phys 20:722-725.
[20]. J.Fleming (1976) Frontier orbital and organic chemical reaction Wiley,New York.
[21]. S.Wold (1991) Quant Struct Act Rel 10:191-193.
[22]. A. H. Pandith, S . Giri and P.K.Chattaraj.
[23]. J.M.L. Martin and C. Van Alsenoy, GAR2PED, A Program to Obtain a Potential Energy Distribution from a Gaussian Archive Record, University of Antwerp, Belgium, 1995.
[24]. E. D. Glending and F. A.E. Glending, A.E. Read, J.E. Carpenter and F. Weinhold,NBO 6.0.
[25]. A.E. Reed, LA. Curtiss, F. Weinhold, Chem. Rev.88 (1988)899.
[26]. B.M. Giuliano, I. Reva, R. Fausto, J. Phys. Chem. A 114 (2010) 2506–2517.
[27]. J.M.L.Martin, C.V. Alsenoy, Gar2PED, University of Antwerp, Antiwerp, 1995.
[28]. C.F. Matta, R.J. Boyd, The Quantum Theory of atom in molecules Willey VHC,Verlag-Gmbh, 2007, P.12 (Chepter1).
[29]. U.Koch, P. Popelier, J. Phys. Chem. A99 (1995) 9747.
[30]. R.F.W. Bader, J. R. Cheeseman, In AIMPAC Ed., (2000).
[31]. E.Runge, E.K.U. Gross, Phys. Rev.Lett.52 (1984) 997-1000.1208
[32]. M.E. Casida, K.C. Casida, D.R. Salahub, Int. J. Quent. Chem. 70 (1998)933-941.
[33]. D Jackuemin, E.A. Perpete, J.Mol. Struct. Theochem 804 (2007)31.
[34]. P.Politzer and J.S. Murray,Theor. Chem. Acc, 108-134(2002).(electrostatic potential).
[35]. J.M.L. Martin and C. Van Alsenoy, GAR2PED, A Program to Obtain a Potential Energy.Distribution from a Gaussian Archive Record, University of Antwerp, Belgium, 1995
[36]. L. Szentpaly, S. Liu, J. Am. Chem.Soc. 121 (1999) 1922.
[37]. P.K. Chattaraj, S. Giri, J. Phys. Chem.A 111 (2007) 11116.
[38]. J.M.L. Martin and C. Van Alsenoy, GAR2PED, 1995.
[39]. Lee, W. Parr, R.G. Parr (1988) Phy Rev37:785-789.
[40]. M.J. Frisch, et al., Gaussian 09, Revision C.02, Gaussian, Inc., Wallingford, CT.

Supplementary Information

S1-Experimental ^{1}H- NMR spectra.

S2-Optimized structural parameters (bond length, bond angles, and dihedral angles).

Figure Captions

Figure 1. Optimized geometry for the lowest energy conformer of abacavir.

Figure 2. Correlation between calculated and experimental NMR chemical shifts.

Figure 3. The experimental and theoretical UV–Visible spectrum of abacavir.

Figure 4. Molecular orbital plots for high oscillator strength electronic excitations in abacavir.

Figure 5. Experimental FTIR and theoretical IR spectra for abacavir.

Figure 6. Molecular graph of abacavir with bond critical points (green dots) and ring critical points (red dots) using AIM program.

Figure 7. Molecular electrostatic potential (MESP) map of abacavir.

Comparison between experimental and calculated electronic transitions for abacavir: *E* /eV, oscillatory strength (*f*), (λ_{max} / nm) at TD–DFT/B3LYP/6–31G(d,p) level.

S.No.	Excitation	*E* (eV)	(*f*)	λ_{max} calcd.	λ_{max} exp.	% contribution	Assignment
1	76→77 (H→L)	4.6575	0.2231	286.20	306	56.23 55.23	$\pi\rightarrow\pi^*$
2	76→79 H→L+2	5.1538	0.1128	240.57	246	76.12 23.88	π→π*
3	75→77 H-1→L	5.6913	0.2491	217.85		67.96 32.04	σ→σ*
4	75→79 H+1→L-2	6.3692	0.1277	194.66		63.23 37.37	σ→π*
5	73→78 H-3→L+1	7.1158	0.2124	174.24		70.31 29.69	n→σ*
6	70→78 H-6→L-1	7.2345	0.1443	171.38		64.41 34.56	n→σ*

Table-1

Calculated ε_{HOMO}, ε_{LUMO}, energy band gap ($\varepsilon_L - \varepsilon_H$), chemical potential ($\mu$), electronegativity ($\chi$), global hardness ($\eta$), global softness ($S$), global electrophilicity index (ω) for compound.

Fig.	ε_H	ε_L	$\varepsilon_L - \varepsilon_H$	χ	μ	η	S	ω
(1)	-5.0817	-0.0095	5.0912	2.5456	-2.5456	2.5361	0.1971	1.2776

ε_H, ε_L, $\varepsilon_L - \varepsilon_H$, χ, μ, η, ω (in eV) and S (in eV^{-1})

Table-2

Experimental and calculated (selected) vibrational wavenumbers of monomer using B3LYP/6-31G(d,p) and their assignments [harmonic wavenumbers (cm^{-1}), IR_{int} ($Kmmol^{-1}$)].					
Mode No.	**Wave number unscaled**	**Wave number scaled**	**Exp. Waven umbers**	**Exp. intensity**	**Assignment (PED) ≥ 5 %**
111	3707	3562	3467	42.09	ν(N7H39)(52) -ν(N7H38)(48)
110	3571	3431		74.54	ν(N7H38)(52) ν(N7H39)(48)
109	3548	3409		57.78	ν(N2H31)(99)
108	3482	3345	3299	0.92	ν(O1H37)(100)
107	3278	3150		1.2	ν(C20H36)(52)-δ(R2)(33)δ(R2)(10) ν(N4C20)(5)
106	3271	3143	3104	12.98	ν(C9H23)(47)-ν(C9H24)(33)-ν(C10H25)(8) ν(C10H26)(6)
105	3260	3132		6.04	ν(C15H33)(86) ν(C14H32)(11)
104	3250	3122		3.48	ν(C10H25)(44) -ν(C10H26)(35) ν(C9H23)(9)-ν(C9H24)(6)
103	3219	3093		4.3	ν(C14H32)(85) -ν(C15H33)(12)
102	3177	3052		5.89	ν(C9H24)(43)ν(C9H23)(31) (δ-C8H23H24)(10) ν(C8H22)(5)
101	3166	3042	3018	20.79	ν(C8H22)(43) ν(C10H26)(19) ν(C10H25)(11) -(ρ-C8C10N2)(8) -ν(C9H24)(6)
100	3164	3040		9.31	ν(C8H22)(35) -ν(C10H26)(24) -ν(C10H25)(24) -δ(C8H25H26)(6) -(ρ-C8C10N2)(5)
99	3156	3033		10.41	ν(C12H29)(66)-ν(C12H28)(32)
98	3104	2982	2970	28.12	ν(C12H28)(60) ν(C12H29)(33)
97	3080	2959		21.95	ν(C19H35)(38) -ν(C13H30)(37) -δ_S(C13C19 O1)(8)
96	3060	2940	2890	17.31	ν(C11H27)(81) δ(N3C14H27)(7)
95	3058	2938		7.25	ν(C13H30)(39) ν(C19H35)(38) -δ_S(C13C19 O1)(10)
94	2986	2869	2850	66.03	ν(C19H34)(75) -δa_S(C13C19O1)(10) ν(C19H35)(7)
93	1691	1625	1630	1.98	δ (NH2)(58) δ(R1)(7)
92	1662	1597	1590	337.96	(δtrigonal-R3)(58) -(δas-R3)(30) (δsc-NH2)(6)
91	1630	1566	1570	467.79	(δas-R3)(71) δ(R2)(16)
90	1598	1536		3.91	ρ–(C13H35O1)(30) -δ(C17N3C17)(14) -(δtrigonal-R3)(9)-δ(R2)(8) δ_S(C13C19 O1)(8) – δas(C19C13H34)(8) -ν(C17C18)(7) ρ–(C13C19H35)(5)
89	1594	1532	1530	352.3	δ(C17N3C17)(28)(δtrigonal-R3)(21) δ(R2)(17) ν(C17C18)(17) - ν(N6C17)(6)
88	1540	1480	1471	180.38	δ(C17N3C17)(42) -δtrigonal-(R3)(30) ν(C17C18)(11) -δ(R2)(5)
87	1537	1477	1470	31.95	δ(C12H28H29)(71) -ν(C17C18)(7) -δ(C17N3C17)(5)
86	1524	1465	1450	17.67	δas-(R3)(23)-δ(C17N3C17)(20) -δ(C8H25H26)(14) -(δ-C8H23H24)(10) -ν(C17C18)(8) -ω–(C8C10H25)(7) -(ω-C9C8H23)(5)
85	1508	1449		10.21	δas-(R3)(38) δ-(C8H23H24)(12) δ(R2)(10)ω-(C9C8H23)(9) -δ(C8H25H26)(8)-δtrigonal-(R3)(6) -ω– (C8C10H25)(5)
84	1500	1441	1435	192.01	δas-(R3)(56)-δ(C17N3C17)(15)δ(R2)(10) -ν(C17C18)(5)
83	1489	1431	1420	86.14	δ(C17N3C17)(54)ν(N5C16)(11)δ(R2)(8) ν(C17C18)(8)
82	1468	1411		8.21	δas(C13C19O1)(19) δ(C17N3C17)(18) δs(C13C19O1)(13) δ(C19O1C37)(11) -ν(C13C19)(6) (δtrigonal-R3)(5) ν(C17C18)(5)
81	1454	1397	1380	24.45	δ(R2)(50) δ(C17N3C17)(17) ν(N4C20)(13) δ(R2)(11)
80	1410	1355	1347	29.18	δ(C17N3C17)(34) -ν(N4C20)(29) -(δas-R3)(10) ν(C17C18)(8)-δ(R2)(5)
79	1400	1345		8.97	δ(C17N3C17)(40) -ν(N4C20)(13) -(δas-R3)(11) ν(C17C18)(7)
78	1388	1333	1325	166.09	δ(C17N3C17)(38)-(δas-R3)(15) -δ(R2)(11)(ρ-C8C10N2)(9) ν(C17C18)(9)
77	1380	1326	1315	38.54	δ(C17N3C17)(73) -(δas-R3)(7) ν(C17C18)(6)
76	1366	1313		25.92	δ(C17N3C17)(73) ν(C17C18)(7) -(δas-R3)(6)
75	1345	1292		15.82	ω–(C11C12H29)(22) -ν(C17C18)(15) -δ(C11C14H32)(10) -δ(C17N3C17)(8) -δ(C14C15H33)(8)ν(N5C21)(7)-δ(C13C15H30)(6) δ(C11C14H27)(5)
74	1339	1286	1270	28.63	ν(C17C18)(42)δ(C17N3C17)(13) -ν(N5C21)(12) -δ(R2)(9)(δas-R3)(5)
73	1331	1279	1268	87.58	ν(C17C18)(37) -δ(R2)(22) -ν(N5C21)(11) δ(R2)(11)(δas-R3)(6)

72	1322	1271		10.21	δ(R2)(15) -δ(R2)(14) -δ(C17N3C17)(14) (δas-R3)(10) ν(C17C18)(6)
71	1282	1232	1225	59.36	ν(N4C20)(20)δ(R2)(16)(δtrigonal-R3)(15) δ(C17N3C17)(11)ν(C17C18)(11) ν(N6C17)(7) -(δas-R3)(7) -ν(N4C18)(6)
70	1278	1228		18.07	δ(R2)(53)δ(C17N3C17)(11)(δtrigonalR3) (8)
69	1270	1220	1209	34.71	δ(C17N3C17)(38)δ(R2)(37)ν(N5C16)(7) δ(R2)(5)
68	1248	1199		34.29	δs(C13C19O1)(36) -δas(C13C19O1)(27) -δ(C15C19H30)(8) -ρ–(C13H35O1)(7) -δas(C19C13H34)(7)δ(C19O1C37)(5) -δ(C13C15H30)(5)
67	1243	1195		11.72	δ(R2)(45) -δ(R2)(15) -(δtrigonal-R3)(13) -ν(C17C18)(7) -ν(N3C17)(6)
66	1221	1173		1.32	δtrigonal-(R3)(57) -δ(C17N3C17)(21) δ(R2)(6)
65	1215	1168	1132	35.64	δ(R2)(40) -ν(C17C18)(25) δ(C17N3C17)(19)
64	1205	1158		3.97	(δtrigonal-R3)(29)δ(R2)(16) -ν(C17C18) (14) δ(R2)(11) -t–(C8C9H23)(5)
63	1191	1145		3.37	ν(C9C10)(20) t–(C8C10N2)(15) ν(C8C10)(14)ν(C8C9)(11) -ρ-(C9C8H23)(8) ρ-(C8C10C25)(5)
62	1171	1125	1130	14.95	δ(R2)(31)δ(C17N3C17)(30)-δ(R2)(12) -ν(N3C20)(9) ν(N3C17)(8)
61	1159	1114		6.99	δ(C17N3C17)(48)δ(R2)(16) δ(C14C15H33)(9)-δ(C11C14H32)(8)
60	1142	1097		1.17	δ-(C10N2H22)(19)δ(C17N3C17)(18) -t– (C8C10N2)(9) -ω–(C8C10H25)(8)
59	1113	1069		5.98	δtrigonal-(R3)(34)as(C19C13H34)(11) -δ(C17N3C17)(9) δ(C13C15H30)(5)
58	1107	1063		3.36	δtrigonal-(R3)(41) -δ(C17N3C17)(31) δ(R2)(17)
57	1099	1056		5.77	δtrigonal-(R3)(41) -δ(C17N3C17)(23) δ(R2)(21) ν(N5C21)(5)
56	1080	1037		6.7	δ(R2)(28) -δ(C13C15H30)(12)(δtrigonal-R3)(10)δ(C11C14H27)(8)-δ(R1)(6)-ν(C11C12)(5)
55	1077	1035	1020	25.29	δ(R2)(41) -ν(C9C10)(13)(δtrigonal-R3)(7)
54	1057	1016		4.53	δ(C17N3C17)(67) -(δas-R3)(13) -(δtrigonal-R3)(8)
53	1050	1009		12.08	δ(C17N3C17)(69) -(δtrigonal-R3)(20)
52	1028	988.1		10.25	δ(R2)(35)(δas-R3)(24)-δ(R2)(18)
51	1010	970.4	962	82.56	δ(R2)(20)ν(O1C19)(19)(δas-R3)(7) -(ρ–C13C19H35)(6)-ν(C13C19)(5)-δ(C15C19H30)(5) -δ(C11C14H27)(5)
50	1004	964.5		7.53	(ω–C153H33)(35) -ω–(C14H32)(33) δ(C17N3C17)(7)
49	990	951.4	955	14.71	δ(R2)(32)δ(C13C15H30)(18) ν(C11C14)(10) -ν(C12C13)(9)
48	967	929.4		46.2	δas-(R3)(38) -δ(R2)(30)δ(R2)(12) -δ(C17N3C17)(9)
47	957	919.6		1.33	δas-(R3)(54) -δ(R2)(13) δ(R2)(9)
46	944	907		4.32	δ(C17N3C17)(50)(δas-R3)(12) -(δtrigonal-R3)(9) -ν(N5C21)(6) δ(R2)(5)
45	912	876.2		18.5	R3-(Puckering)(28) δoop-(C16N2)(16) -δ(R2)(13) -τ-(R2)(12) τ-(R2)(6) δ(R2)(6) δtrigonal-(R3)(5) -δas-(R3)(5)
44	905	869.6	859	18.09	δ(R2)(52) -δ(R2)(23) δ(C17N3C17)(10)
43	849	816		7.37	δtrigonal-(R3)(36)δ(R2)(28) -δ(C17N3C17)(15)-δ(R2)(9)
42	836	803.6	812	4.24	δtrigonal-(R3)(45) -ω-(NH2)(11) δ(R2)(11)
41	835	801.8		27.22	δtrigonal-(R3)(29) -ω-(C20H36)(24) -δas-(R3)(9) δ(R2)(9)
40	829	796.9		6.03	(δtrigonal-R3)(65)δ(R2)(12) -δ(C17N3C17)(7)
39	823	790.3		1.15	δtrigonal-(R3)(60)δ(R2)(14)δ(R2)(7) ν(C17C18)(6)δas-(R3)(5)
38	799	767.6	757	45.14	δ(R2)(30)(δtrigonal-R3)(22) -(δas-R3)(13) ω– (C14H32)(7) δ(C17N3C17)(6)
37	792	761		18.89	δ(R2)(37)(δtrigonal-R3)(31) -δ(R1)(11)
36	786	754.8	748	37.98	(δoop-C21N7)(61)(R3-Puckering)(14) -(t– R3)(11) -(t– R3)(5)
35	778	747.9		0.79	δ(C17N3C17)(26)δ(R2)(25)(δas-R3)(10) ν(C9C10)(6)
34	766	736.3		2.86	(δas-R3)(35)-δ(R2)(25)δ(R2)(15) -δtrigonal-(R3)(8)
33	749	719.4		2	δ(R2)(22)(δoop-C16N2)(17) δ(C17N3C17)(16)-(τ-R2)(9)-(t–R3)(9) δ(R2)(7)
32	739	710.4		5.27	δ(C17N3C17)(61) δ(R2)(15) δ(R2)(14)
31	688	661.2		16.93	δ(C17N3C17)(70) δ(R2)(12) -(δas-R3)(10)
30	678	651	657	26.99	δ(C17N3C17)(64)-(δas-R3)(11) δ(R2)(9)(τ-R2)(6) τ-(R2)(5)
29	637	612.4		1.2	δas-(R3)(66)-δtrigonal-(R3)(14) δ(C17N3C17)(6) δ(R2)(6) δ(R2)(6)
28	584	560.9		2.33	δ(C17N3C17)(51) -δas-(R3)(46)

27	573	550.8	535	89.49	ω–(N2H31)(31)τ-(N2C16)(30)δas-(R3)(10) δ(C17N3C17)(6) δ(R2)(5)
26	540	518.4		1.14	τ-(N7C21)(82) -δas-(R3)(9)
25	518	498.1		3.02	δ(R2)(20)(δas-R3)(19)ν(N3C17)(10)(δas-R3)(10)-δ(C17N3C17)(8) -ν(C17C18)(8) ν(N6C17)(6) ν(N4C18)(5)
24	474	455.4		2.57	δ(C17N3C17)(55) -(δas-R3)(36)
23	458	440.2		3.36	δas-(R3)(60) -δ(C17N3C17)(32) δ(R2)(5)
22	449	431.7		15.51	δ(C17N3C17)(52) -δas-(R3)(20) δ(R2)(7) δ(R2)(5)
21	440	422.4		15.56	δas-(R3)(41) δ(R2)(29) -δ(C17N3C17)(10)

Table-3

Selected reactivity descriptors as Fukui functions (f_k^+, f_k^-), local softnesses (s_k^+, s_k), local electrophilicity indices (ω_k^+, ω_k^-) for compound, using Hirshfild atomic charges.

sites	f_k^+	s_k^+	ω_k^+	sites	f_k^-	s_k^-	ω_k^-
C8	0.0215	0.292525	0.029866	O1	0.0205	0.278919	0.028477
C9	0.0345	0.4694	0.047924	N2	0.0957	1.302075	0.132937
C10	0.0465	0.63267	0.064593	N3	0.0249	0.338784	0.034589
C16	0.0815	1.108873	0.113212	N4	0.0529	0.719747	0.073483
C17	0.0184	0.250347	0.025559	N5	0.0280	0.380962	0.038895
C20	0.1399	1.903451	0.194335	N6	0.0929	1.263979	0.129047
C21	0.0433	0.589131	0.060148	N7	0.1511	2.055836	0.209893

f_k^+, f_k^- (in e); s_k^+, s_k^- (in eV^{-1}) and ω_k^+, ω_k^- (in eV).

Table-4

Table-7 Second–order perturbation theory analysis of the Fock matrix in NBO basis for (3): Selected donor (Lewis) and acceptor (non–Lewis) orbitals, percentage electron density over bonded atoms (ED_A, ED_B in %), NBO hybrid orbitals of bonded atoms and stabilization energy of various intramolecular interactions ($E^{(2)}$).

Donor (i)			Acceptor (j)			$E^{(2)}$ (kcal/ mol)
Orbital / lp (occupancy)	ED_A, % ED_B, %	NBO hybrid orbitals	orbital (occupancy)	ED_A, % ED_B, %	NBO hybrid orbitals	
π (N6–C21) (1.77385)	58.88 41.12	0.7970 $(sp^{1.93})_N$ 0.6040 $(sp^{1.84})_C$	π *(N5–C16) (0.04203)	41.76 58.24	0.6504 $(sp^{1.78})_N$ -0.7596 $(sp^{2.12})_C$	5.49
π(N6-C21) (1.77385)	67.91 32.09	0.7971$(sp^{1.93})_N$ 0.6038$(sp^{1.84})_C$	π*(C17–C18) (0.02409)	49.92 50.08	0.6504 $(sp^{1.72})_C$ -0.7596 $(sp^{2.05})_C$	30.50
π (C17-C18) (1.96891)	50.08 49.92	0.7065 $(sp^{1.00})$ -0.7077$(sp^{2.55})_C$	π*(N4–C20) (0.40430)	49.92 50.08	0.7161$(sp^{1.83})_N$ -0.6980$(sp^{1.82})_C$	17.71
π(N7–H39) (1.98660)	69.39 30.61	0.6980$(sp^{2.67})_N$ 0.7161$(sp^{0.00})_H$	π*(N5–C21) (0.03706)	41.10458 .90	0.5532 $(sp^{1.89})_N$ -0.8330 $(sp^{1.88})_C$	4.28
π(O1-C19) 1.99402	66.86 33.14	0.7596$(sp^{2.37})_O$ 0.5756$(sp^{3.60})$c	(O1-C19) 0.01291	33.14 66.86	0.5756 $(sp^{2.37})_O$ -0.8177 $(sp^{3.60})$c	4.51
π(N4–C20) (1.90374)	58.54 41.46	0.7651 $(sp^{1.83})_N$ 0.6439 $(sp^{1.82})_C$	π*(C17-C18) (0.04203)	49.92 50.08	0.64398$(sp^{1.72})_C$ 0.6462 $(sp^{2.05})_C$	15.98
π(N5–C16) (1.97676)	58.24 41.76	0.7631 $(sp^{1.78})_N$ 0.6462$(sp^{2.21})_C$	π*(C17-C18) (0.04203)	49.92 50.08	0.6439 $(sp^{1.72})_C$ -0.7651 $(sp^{2.05})_C$	6.66
π (C17-C18) (1.96891)	50.08 49.92	0.7065 $(sp^{1.93})$ -0.7077$(sp^{2.55})_C$	π *(N5–C16) (0.03477)	49.92 50.08	0.5350 $(sp^{1.78})_N$ -0.8449$(sp^{2.22})_C$	32.34
π (C17-C18) (1.96891)	50.08 49.92	0.7065 $(sp^{1.93})$ -0.7077$(sp^{2.55})_C$	π *(N6–C21) (0.03223)	49.92 50.08	0.6259$(sp^{1.94})_N$ -0.7799$(sp^{1.81})_C$	9.01
π (C14-C15) (1.76134)	50.19 49.81	0.7057 $(sp^{1.59})$ -0.7085$(sp^{1.64})_C$	σ*(N3–C11) (0.27529)	48.63 51.37	0.5939$(sp^{1.87})_N$ -0.8045$(sp^{3.55})_C$	4.12
σ (N3-C20) (1.98369)	64.25 35.75	0.8016$(sp^{2.14})_N$ 0.5979$(sp^{2.30})_C$	σ*(N4-C20) (0.00662)	41.31 58.69	0.5979 $(sp^{1.00})_N$ -0.8016$(sp^{1.00})_C$	5.32
σ (N4-C20) (1.90374)	58.54 41.46	0.7651$(sp^{1.83})_N$ 0.6439$(sp^{1.82})_C$	σ*(C16-C18) (0.03888)	50.52 49.48	0.64398$(sp^{1.65})_C$ 0.6462$(sp^{1.98})_C$	5.59
σ (N6–C17) (1.97952)	57.70 42.30	0.6933 $(sp^{1.87})_N$ 0.7206$(sp^{1.86})_C$	σ *(N7–C21) (0.03479)	40.10559 .90	0.6618$(sp^{1.67})_N$ -0.7497$(sp^{2.34})_C$	4.27
σ(N6–C21) (1.77385)	58.88 41.12	0.6933$(sp^{1.93})_N$ 0.7206$(sp^{1.84})_C$	σ*(N3–C17) (0.04549)	37.15562 .85	0.6504 $(sp^{2.01})_N$ -0.7596 $(sp^{2.57})_C$	7.06
π(N7–H39) (1.98660)	69.39 30.61	0.6980$(sp^{2.67})_N$ 0.7161$(sp^{0.00})_H$	π*(C19–H34) (0.02662)	41.57 58.43	0.5532 $(sp^{3.17})_C$ -0.8330 $(sp^{0.00})_H$	146.0
σ (N2-H31) (1.98156)	70.56 29.44	0.8400$(sp^{1.70})_N$ 0.5426$(sp^{2.35})_H$	σ*(N5-C16) (0.46431)	31.97 68.03	0.6462 $(sp^{1.78})_N$ -0.7631$(sp^{2.12})_C$	5.14
σ (N7–C21) (1.98991)	59.90 40.10	0.7218$(sp^{1.67})_C$ 0.6921 $(sp^{2.34})_C$	σ * (C19-C34) (0.02662)	41.57 58.43	0.6333 $(sp^{1.67})_C$ -0.7739 $(sp^{2.34})_C$	70.79
σ(N7–C21) (1.98991)	59.90 40.10	0.7218 $(sp^{1.67})_C$ 0.6921 $(sp^{2.34})_C$	σ *(C19-H34) (0.02662)	41.57 58.43	0.6333 $(sp^{1.67})_C$ -0.7739 $(sp^{2.34})_H$	34.85
σ(N7–C21) (1.98991)	59.90 40.10	0.7892 $(sp^{1.67})_N$ 0.6141 $(sp^{2.34})_C$	σ *(C20-H36) (0.02171)	40.20 59.80	0.6333 $(sp^{1.91})_C$ -0.7739 $(sp^{0.00})_H$	16.46
σ (N7–C21) (1.98991)	59.90 40.10	0.7089$(sp^{1.67})_C$ 0.7053$(sp^{2.34})_C$	π*(C20–C36) (0.02171)	40.20 59.80	0.6333 $(sp^{1.91})_C$ -0.7739 $(sp^{0.00})_C$	4.15

σ(N7–H38) (1.98676)	69.54 30.46	0.7055($sp^{2.64}$)c 0.7087($sp^{0.00}$)c	σ*(N6-C21) (0.03691)	41.12 62.02	0.5519 ($sp^{1.00}$)$_N$ -0.8339 ($sp^{1.00}$)$_C$	4.17
σ(N7–H38) (1.98676)	69.54 30.46	0.7055($sp^{2.64}$)c 0.7087($sp^{0.00}$)c	σ*(C19–H34) (0.02662)	41.57 58.43	0.5519 ($sp^{3.17}$)$_C$ -0.8339 ($sp^{0.00}$)$_H$	66.71
σ(N7–H39) (1.98660)	69.39 30.61	0.7134($sp^{2.67}$)$_N$ 0.7008 ($sp^{0.00}$)$_H$	σ*(C19–H35) (0.02444)	47.62 52.38	0.5532 ($sp^{3.12}$)$_C$ 0.8330 ($sp^{0.00}$)$_H$	21.13
σ(N7–H39) (1.98660)	69.39 30.61	0.6500($sp^{2.65}$)$_N$ 0.7599($sp^{0.00}$)$_H$	σ *(C20-H36) (0.02171)	40.20459 .80	0.5532 ($sp^{1.91S}$)$_C$ -0.8330 ($sp^{0.00}$)$_H$	33.74
σ(C8–C9) (1.95427)	50.88 49.12	0.7799($sp^{2.55}$)$_C$ 0.6259($sp^{0.00}$)$_C$	σ*(C8–C10) (0.02809)	49.09 50.91	0.7009 ($sp^{1.87}$)$_C$ -0.7133 ($sp^{2.79}$)$_C$	5.84
σ (C8-C9) (1.95427)	50.88 49.12	0.7799 ($sp^{3.26}$)$_C$ 0.6259 ($sp^{3.48}$)$_C$	σ *(C9-C10) (0.02254)	49.12 50.88	0.7599($sp^{3.42}$)$_C$ -0.6500($sp^{3.45}$)$_C$	5.52
σ (C8-C10) (1.95591)	50.91 49.09	0.7007($sp^{3.42}$)$_C$ -0.7135($sp^{3.45}$)$_C$	σ*(C8–C9) (0.27529)	49.09 50.91	0.5939($sp^{3.26}$)$_C$ -0.8045($sp^{3.48}$)$_C$	6.08
σ (C8-C10) (1.95591)	50.91 49.09	0.7007 ($sp^{2.55}$) -0.7135($sp^{2.55}$)$_C$	σ*(C9–C10) (0.20833)	49.09 50.91	0.7363($sp^{3.57}$)$_C$ -0.6767($sp^{3.51}$)$_C$	5.83
σ (C9-C10) (1.96153)	49.45 50.55	0.7110 ($sp^{2.55}$) -0.7032($sp^{2.55}$)$_C$	σ*(C8–C9) (0.2752)	50.55 49.45	0.5939($sp^{3.26}$)$_C$ -0.8045($sp^{3.48}$)$_C$	5.37
σ (C9-C10) (1.96153)	49.45 50.55	0.7110 ($sp^{2.55}$) -0.7032($sp^{2.55}$)$_C$	σ*(C8–C10) (0.15073)	50.55 49.45	0.8133($sp^{1.87}$)$_C$ -0.5819($sp^{2.79}$)$_C$	5.85
σ (C11-C14) (1.97149)	52.12 47.88	0.6919 ($sp^{2.52}$) -0.7220($sp^{2.30}$)$_C$	σ*(C15–H33) (0.27529)	47.86 52.12	0.5939($sp^{2.24}$)$_C$ -0.8045($sp^{0.00}$)$_H$	4.56
σ (C11-H27) (1.96603)	60.44 39.56	0.6290 ($sp^{3.57}$) -0.7774($sp^{0.00}$)$_C$	σ*(N3–C17) (0.14721)	39.56 60.44	0.8135($sp^{2.01}$)$_N$ -0.5816($sp^{2.57}$)$_C$	4.92
σ (C13-H15) (1.97263)	51.47 48.53	0.6966 ($sp^{2.76}$) -0.7175($sp^{2.21}$)$_C$	σ*(C14–H32) (0.20833)	39.37 60.63	0.7363($sp^{2.22}$)$_C$ -0.6767($sp^{0.00}$)$_H$	4.79
σ (C17-C18) (1.96891)	50.08 49.92	0.7065 ($sp^{2.76}$) -0.7077($sp^{2.21}$)$_C$	σ *(N2–C16) (0.20833)	49.92 50.08	0.7363($sp^{1.70}$)$_N$ -0.6767($sp^{2.35}$)$_C$	4.14
σ (C17-C18) (1.96891)	50.08 49.92	0.7065 ($sp^{1.00}$) -0.7077($sp^{2.55}$)$_C$	σ *(N3–C11) (0.34531)	49.92 50.08	0.7173 ($sp^{1.87}$)$_N$ -0.6967 ($sp^{3.85}$)$_C$	5.82
lp_1(N2) (1.72048)		($sp^{61.81}$)$_N$	π *(N5–C16) (0.46431)	31.97 68.03	0.5654 ($sp^{1.00}$)$_N$ -0.8248 ($sp^{1.00}$)$_C$	56.28
lp_1(N2) (1.72048)		($sp^{61.81}$)$_N$	σ*(C8–C9) (0.04016)	49.12 50.88	0.7009 ($sp^{3.26}$)$_C$ 0.7009 ($sp^{3.48}$)$_C$	5.78
lp_1(N2) (1.72048)		($sp^{61.81}$)$_N$	σ*(C8–H22) (0.03063)	39.19 60.81	0.6260 ($sp^{2.55}$)$_C$ 0.7798($sp^{0.00}$)$_H$	7.55
lp_1(N3) (1.58198)		($sp^{1.00}$)$_N$	σ*(N4–C20) (0.00662)	41.31 58.69	0.6427 ($sp^{1.83}$)$_N$ -0.7661($sp^{1.82}$)$_C$	44.75
lp_1(N3) (1.58198)		($sp^{1.00}$)$_N$	σ*(C11–C12) (0.02135)	48.56 51.44	0.6968 ($sp^{1.00}$)$_C$ -0.7172($sp^{1.00}$)$_C$	4.85
lp_1(N3) (1.58198)		($sp^{1.00}$)$_N$	σ*(C11–C14) (0.02756)	47.88 52.12	0.6919 ($sp^{1.00}$)$_C$ -0.7220(sp)$_C$	4.87
lp_1(N3) (1.58198)		($sp^{1.00}$)$_N$	π*(C17–C18) (0.04203)	49.92 50.08	0.7065 ($sp^{2.14}$)$_C$ 0.7077($sp^{2.30}$)$_C$	39.71
lp_1(N4) (1.92510)		($sp^{1.97}$)$_N$	σ *(N3–C20) (0.03718)	35.75 64.25	0.5979 ($sp^{2.14}$)$_N$ -0.8016 ($sp^{2.30}$)$_C$	7.79
lp_1(N4) (1.92510)		($sp^{1.97}$)$_N$	σ *(C17–C18) (0.04203)	49.92 50.08	0.7065($sp^{1.72}$)$_C$ -0.7077($sp^{2.05}$)$_C$	5.46
lp_1(N5) (1.90346)		($sp^{2.39}$)$_N$	σ *(N2–C16) (1.98499)	60.68 39.32	0.7790 ($sp^{1.70}$)$_N$ 0.6270 ($sp^{2.35}$)$_C$	4.07
lp_1(N5) (1.90346)		($sp^{2.39}$)$_N$	σ *(N6–C21) (1.77385)	67.91 32.09	0.8241 ($sp^{1.00}$)$_N$ 0.5665 ($sp^{1.00}$)$_C$	12.55
lp_1(N5) (1.90346)		($sp^{2.39}$)$_N$	σ *(C16–C18) (1.97178)	49.48 50.52	0.7034 ($sp^{1.65}$)$_C$ 0.7108 ($sp^{1.78}$)$_C$	8.35
lp_1(N6) (1.90598)		($sp^{2.21}$)$_N$	σ *(N5–C21) (1.98353)	58.90 41.10	0.7675 ($sp^{1.89}$)$_N$ 0.6411 ($sp^{1.88}$)$_C$	12.24
lp_1(N6) (1.90598)		($sp^{2.21}$)$_N$	σ *(C17–C18) (1.96891)	50.08 49.92	0.7077($sp^{1.89}$)$_C$ 0.7065($sp^{1.89}$)$_C$	8.52
lp_1(N7) (1.80808)		($sp^{1.94}$)$_N$	π *(N6–C21) (1.98019)	58.88 32.09	0.8241($sp^{1.89}$)$_N$ 0.5665($sp^{1.89}$)$_C$	39.03
lp_1(N7) (1.80808)		($sp^{11.90}$)$_N$	σ *(C19–H34) (1.98627)	58.43 41.57	0.7644 ($sp^{3.70}$)$_C$ 0.6447 ($sp^{0.00}$)$_H$	6.48
lp_1(N7) (1.80808)		($sp^{11.90}$)$_N$	σ *(C20–H36) (1.98529)	59.80 40.20	0.7733 ($sp^{1.91}$)$_C$ 0.6340 ($sp^{1.00}$)$_H$	17.41

Table-5

Selected Lewis orbitals (occupied bond or lone pair) with their NBO hybrids: A, B- bonded atoms, lp-lone pair and (ED,%)-percentage electron density.

Orbital/lp (occupancy)	$ED_A\%$ $ED_B\%$	NBO Hybrid orbitals	s,p, %	Orbital/lp (occupancy)	$ED_A\%$ $ED_B\%$	NBO Hybrid Orbitals
σ (N2-H31) (1.98156)	70.56 29.44	$0.8400(sp^{1.70})_N$ $0.5426(sp^{2.35})_H$	σ*(N5-C16) (0.46431)	31.97 68.03	$0.6462(sp^{1.78})_N$ $0.7631(sp^{2.12})_C$	5.14
σ (N3-C20) (1.98369)	64.25 35.75	$0.8016(sp^{2.14})_N$ $0.5979(sp^{2.30})_C$	σ*(N4-C20) (0.00662)	41.31 58.69	$0.5979(sp^{1.00})_N$ $0.8016(sp^{1.00})_C$	5.32
σ(N6–C21) (1.77385)	58.88 41.12	$0.6933(sp^{1.93})_N$ $0.7206(sp^{1.84})_C$	σ*(N3–C17) (0.04549)	37.15 62.85	$0.6504(sp^{2.01})_N$ $-0.7596\ (sp^{2.57})_C$	7.06
σ (C13-H15) (1.97263)	51.47 48.53	$0.6966\ (sp^{2.76})$ $0.7175(sp^{2.21})_C$	σ*(C14H32) (0.20833)	39.37 60.63	$0.7363(sp^{2.22})_C$ $-0.6767(sp^{0.00})_H$	4.79
σ (O1-C19) 1.99402	66.86 33.14	$0.7596(sp^{2.37})_O$ $0.5756(sp^{3.60})_C$	σ*(O1-C19) 0.01291	33.14 66.86	$0.5756\ (sp^{2.37})_O$ $-0.8177\ (sp^{3.60})_C$	4.51
lp_1(N2) (1.72048)		$(sp^{61.81})_N$	σ*(C8H22) (0.03063)	39.19 60.81	$0.6260\ (sp^{2.55})_C$ $0.7798(sp^{0.00})_H$	7.55
lp_1(N5) (1.90346)		$(sp^{2.39})_N$	σ*(N6C21) (1.77385)	67.91 32.09	$0.8241\ (sp^{1.00})_N$ $0.5665\ (sp^{1.00})_C$	12.55
lp_1(N4) (1.92510)		$(sp^{1.97})_N$	σ*(N3C20) (0.03718)	35.75 64.25	$0.5979\ (sp^{2.14})_N$ $-0.8016\ (sp^{2.30})_C$	7.79

Calculated Dipole moment (μ_0),Polarisability ($I\alpha_0I$),anisotropy of polarisability ($\Delta\alpha$),First hyperpolarisability (β_0) and their component, using B3LYP/6-311G(d,p).

Dipole moment(μ_0)	Polarisability ($\Delta\alpha$)	Hyperpolarisability (β_0)
μ_x = -1.847	α xx 286.64	β_{xxx} -268.50
μ_y= 4.200	α xy 221.08	β_{xxy} 177.25
μ_z= -1.988	α zz 145.56	β_{xyy} 70.24
μ_0= 5.003	$\lvert\alpha_0\rvert$ 25.55	β_{yyy} -404.59
	Δα 361.55	β_{xxz}- -12.39
		β_{xyz} -4.048
		β_{yyz} -20.22
		β_{xzz} 10.761
		B_{yzz} -14.68
		B_{zzz} -21.25
		β_0 16.62
μ_0 in Debye; $I\alpha_0I$ and Δα in esu; β_0 in 10^{-30} esu.		

Table-6

Topological parameters calculated by QTAIM at BCP of N6···H29. All quantities are in a.u.

Atoms	Bond Length	ρ	$\nabla^2\rho$	G	V	H	E
N6···H29	2.6433	0.008371	0.027245	0.005761	-0.004711	0.00105	-0.00238

Table-7

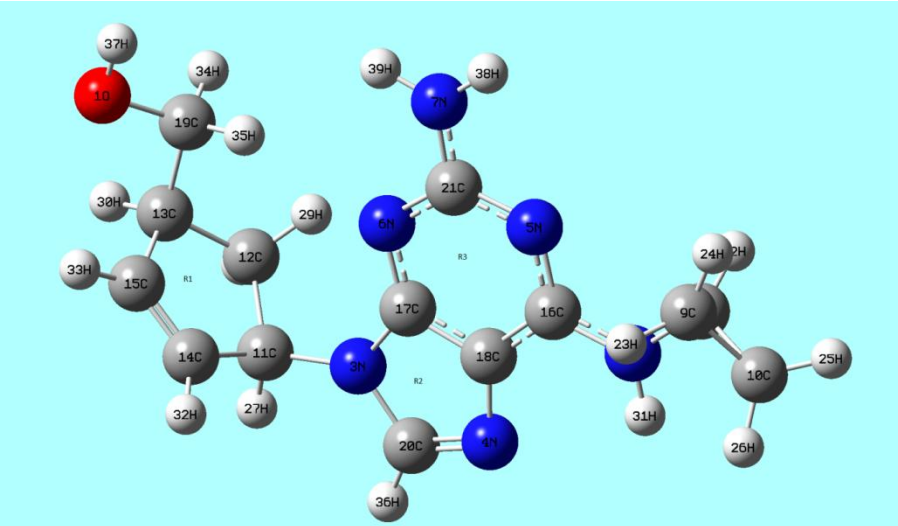

Figure 1. Optimized geometry for the lowest energy conformer of abacavir.

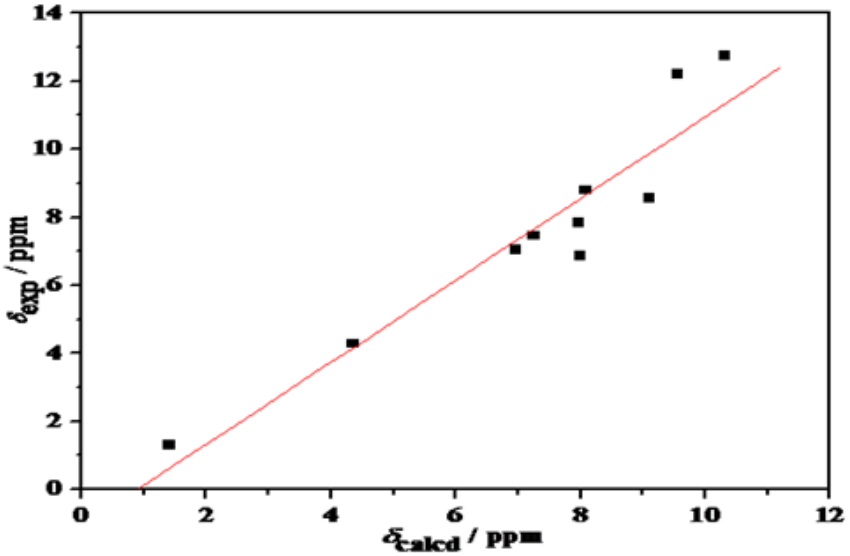

Figure 2. Correlation between calculated and experimental NMR chemical shifts.

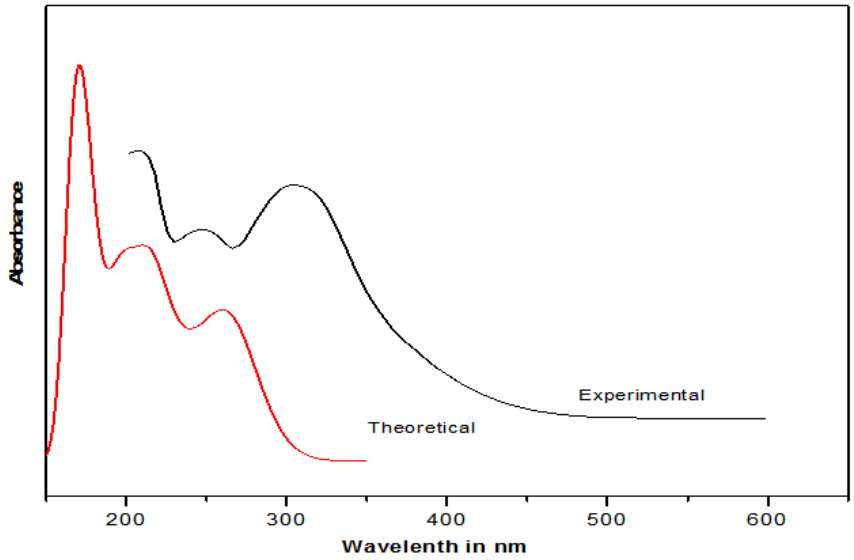

Figure 3. The experimental and theoretical UV–Visible spectrum of abacavir.

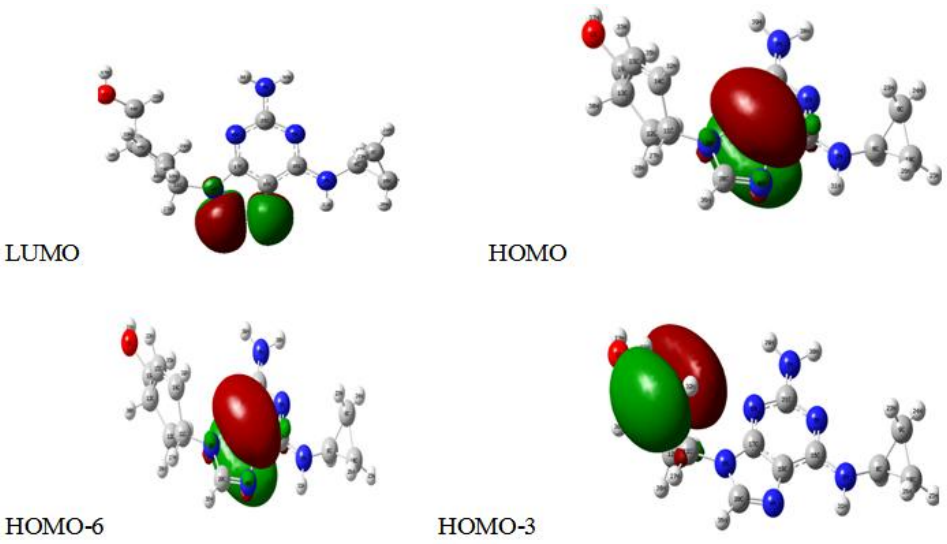

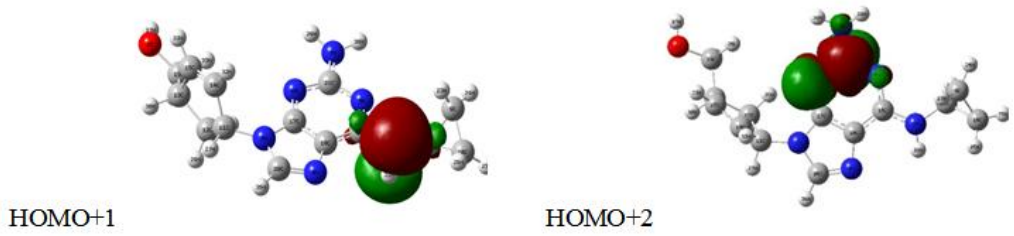

Figure 4. Molecular orbital plots for high oscillator strength electronic excitations in abacavir.

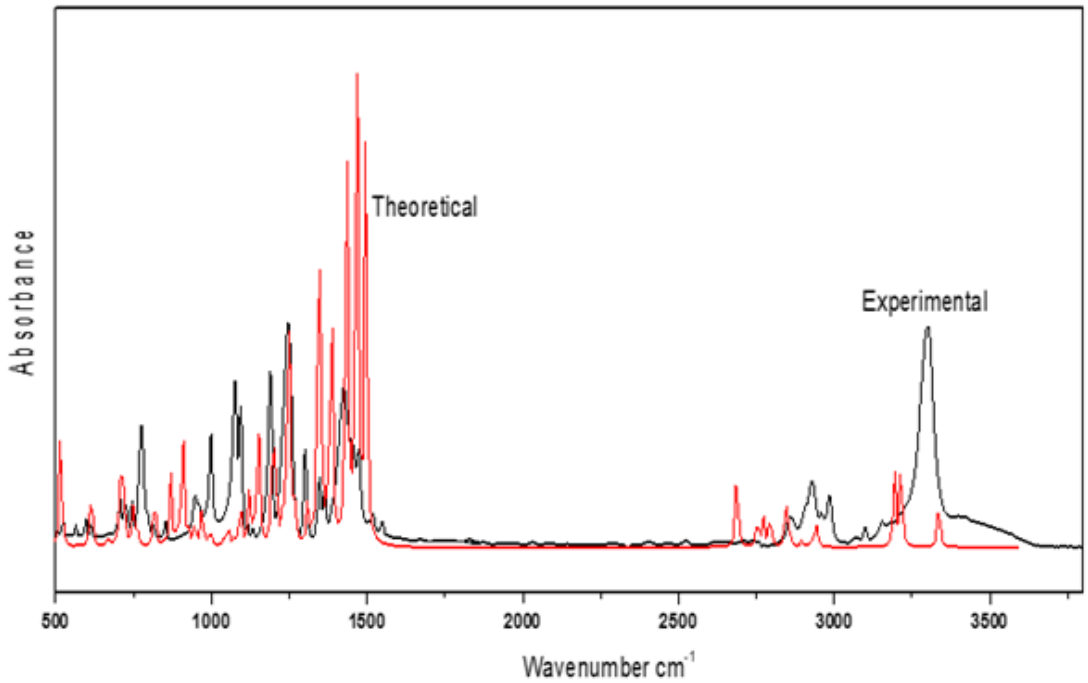

Figure 5. Experimental FTIR and theoretical IR spectra of abacavir.

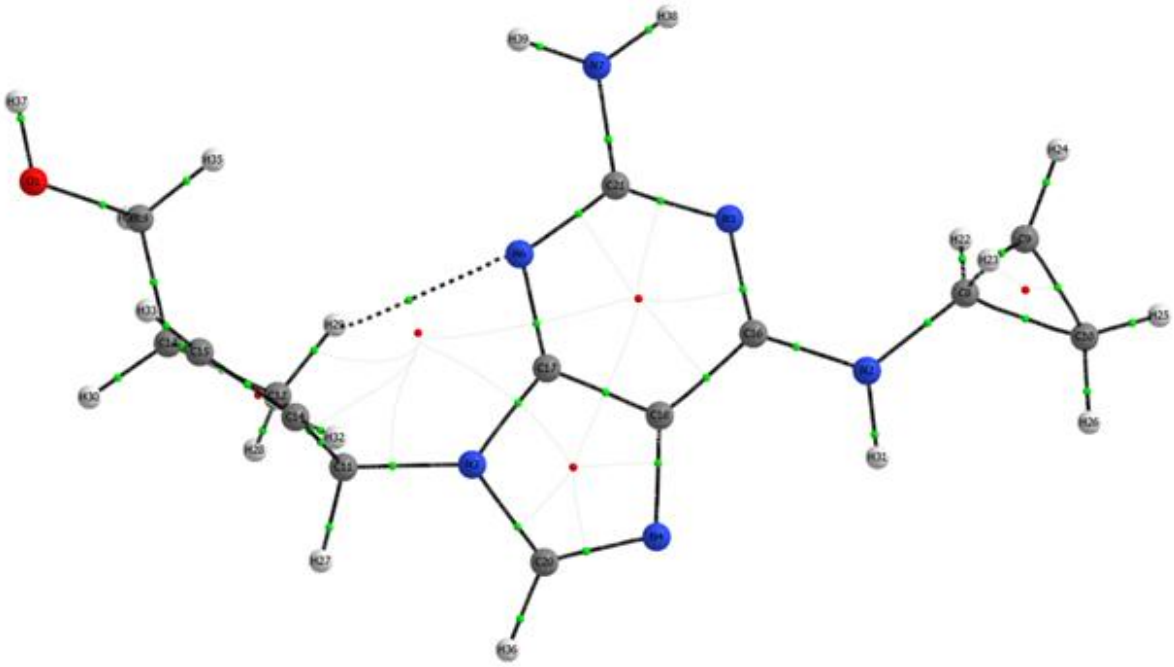

Figure 6. Molecular graph of abacavir with bond critical points (green dots) and ring critical points (red dots) using AIM program.

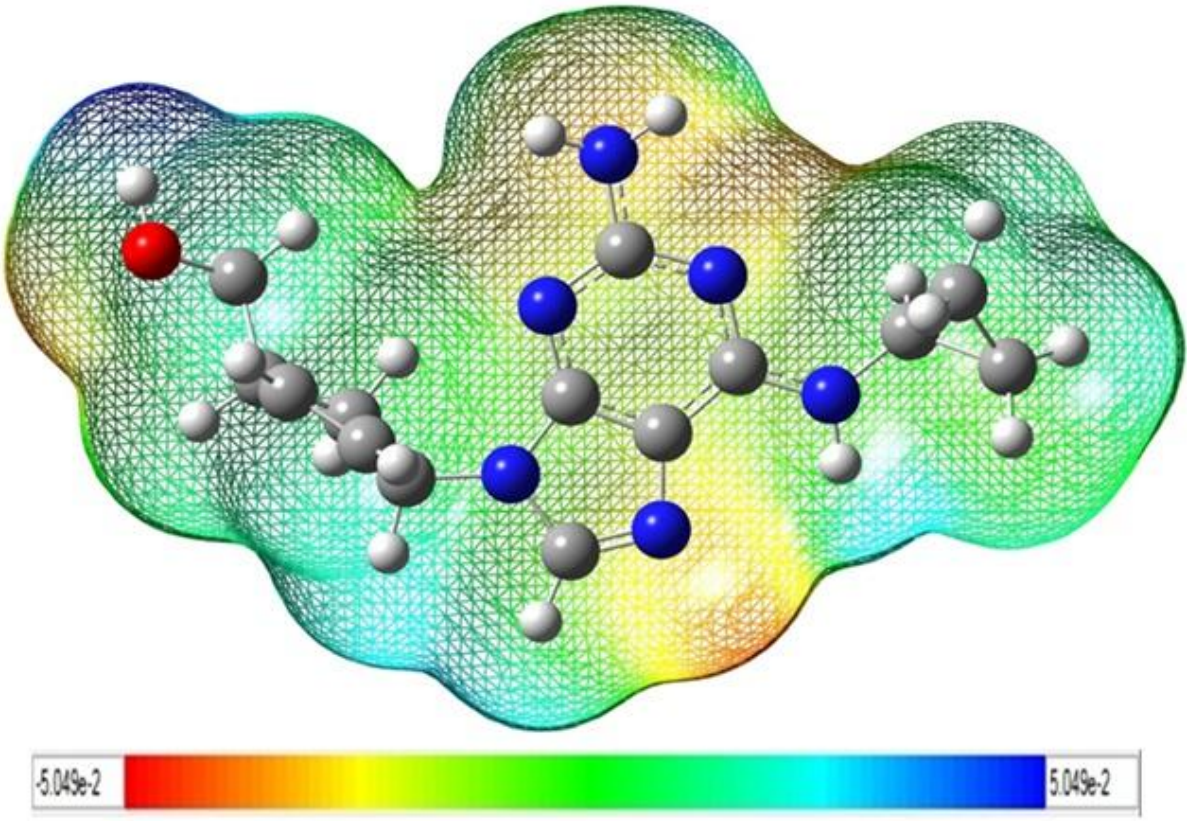

Figure 7. Molecular electrostatic potential (MESP) map of abacavir.